



Published in final edited form as:

Colloid Polym Sci. 2008 ; 286(5): 563–569. doi:10.1007/s00396-007-1805-7.

Size Controlled Synthesis of Monodispersed, Core/Shell Nanogels

William H. Blackburn and L. Andrew Lyon

School of Chemistry and Biochemistry & Petit Institute for Bioengineering and Bioscience, Georgia Institute of Technology, Atlanta, Georgia 30332-0400 (USA)

Abstract

Small, monodispersed nanogels (~ 50-nm radius) were synthesized by free-radical precipitation polymerization and characterized using a suite of light scattering and chromatography methods. Nanogels were synthesized with either *N*-isopropylacrylamide or *N*-isopropylmethacrylamide as the main monomer, with acrylic acid or 4-acrylamidofluorescein as a co-monomer and *N,N'*-methylenebis(acrylamide) as a cross-linker. By varying the surfactant and initiator concentrations, particle size was controlled while maintaining excellent monodispersity. An amine-containing shell was added to these core particles to facilitate subsequent bioconjugation. Successful conjugation of folic acid to the particles was demonstrated as an example of how such materials might be employed in a targeted drug delivery system.

Keywords

nanogels; synthesis; bioconjugation; monodispersity; core/shell

Introduction

Hydrogel colloids, or nanogels, are nanoparticles consisting of randomly oriented, cross-linked, water-soluble polymers. A subclass of nanogels, those based on responsive hydrogels, are able to undergo transitions from a swollen to a deswollen state in response to external stimuli.^{1–8} In recent years, such nanogels have been the focus of research in the areas of drug delivery, biomaterials, biosensing, tissue regeneration, and chemical separations.^{9–17} Some of the most studied nanogels are composed of poly(*N*-isopropylacrylamide) (pNIPAm), a thermoresponsive polymer with a lower critical solution temperature (LCST) of ~31 °C.^{1, 2, 5, 7} Monodispersed nanogels over a wide range of sizes have been synthesized by a number of different methods,^{13, 18, 19} with free-radical precipitation polymerization being the most common.^{7, 18, 20–24}

Perhaps the most interesting behavior of pNIPAm nanogels is the swelling/deswelling of the gels in water upon reaching the lower critical solution temperature (LCST), which occurs around 31 °C. Below this temperature, the particles are hydrophilic and swollen. Above this temperature, the water is expelled, due to an entropically-driven polymer phase separation.^{1, 2, 5, 7} Particles composed of poly(*N*-isopropylmethacrylamide) (pNIPMAm) behave in a similar manner, exhibiting an LCST around 44 °C, with the increased LCST arising from an increase in the rigidity of the pNIPMAm polymer, as is common for methacrylamides.^{25–29} This behavior is important to this work due to the fact that our group has optimized core/shell nanogel synthesis techniques that utilize this LCST behavior to drive the controlled nucleation and growth of the particles.

The focus of the work presented here is related to the size control of a variety of core/shell nanogel constructs. Nanogels to be used for intravenous drug delivery applications such as targeted chemotherapy must be around 100 nm in diameter to be efficient vehicles. Particles of this size do not penetrate into healthy tissues, as pore sizes in the endothelia of blood vessels in most healthy tissues are ~2 nm, while ~6 nm pores are found in postcapillary venules.³⁰ However, the same resistance to particle penetration is not encountered in tumor targeting, as the “leaky” discontinuous tumor vasculature has pore sizes ranging from 100 nm – 780 nm.^{30–32} Typically, this leaky vasculature enables what is called the “enhanced permeability and retention” (EPR) effect, which enables the enhanced deposition of nanoscale delivery vehicles at the site of a solid tumor.^{33–35} Another problem that delivery vehicles encounter is non-specific uptake by the reticuloendothelial system (RES). The surface characteristics of particles can affect uptake by the liver, spleen, and the rest of the RES.^{36, 37} Hydrophilic particles tend to avoid the RES for much longer time periods than hydrophobic particles, thereby permitting longer circulation times, which allow the particles a greater chance to target the site of interest.³⁶ Thus, both size and surface chemistry should be controllable in order to enable the synthesis of effective tumor targeting vehicles.

The nanogels used in this work were synthesized by free-radical precipitation polymerization. In this approach, a free-radical initiator is used to initiate the reaction, while a surfactant is used to stabilize the growing polymer globule. Classically, one would expect that increasing both the surfactant and initiator concentrations would lead to a reduction in particle size.³⁸ Ammonium persulfate (APS) is a free radical initiator, and as the reaction is heated, it creates free radicals and hence growing oligoradicals that act as nucleation sites onto which growing polymer can add. Increasing the initiator concentration leads to more free radicals being formed, and this leads to an increase in number of particles that can potentially be formed. Since the monomer is being consumed by more growing particles under such conditions, the final particle size will be smaller as the same amount of monomer is spread among more particles. Thus, we expect that an increase in the initiator concentration will yield a smaller average particle size. The second control parameter to be explored is that of surfactant concentration. Sodium dodecyl sulfate (SDS) is the surfactant used in the particle syntheses described below. SDS acts to stabilize the growing nuclei against aggregation early in the reaction. Thus, at lower [SDS], particles formed in the early stages of the reaction aggregate to form larger particles, decreasing the number of particles that are formed in a reaction. Conversely, an increase in [SDS] should increase the stability of the early nuclei, allowing them to grow without extensive aggregation and therefore increasing the particle number while decreasing the final particle size. Because of the simplicity of these reaction design considerations, these control parameters are commonly used in dispersion polymerization to control particle size.³⁸ In this study, we demonstrate the ability to synthesize small, monodisperse core/shell nanogel particles. The syntheses are very well controlled, and give us the ability to make a variety of particle sizes. We have also shown the ability to synthesize these small nanogels with different co-monomers thereby producing particles with multiple functionalities. These efforts were undertaken in support of our larger efforts in targeted chemotherapy wherein such synthetic control is critical.

Experimental Section

All materials were purchased from Sigma-Aldrich unless otherwise noted. The monomers *N*-isopropyl acrylamide (NIPAm) and *N*-isopropyl methacrylamide (NIPMAm) were recrystallized from hexane (J. T. Baker) before use. The cross-linker *N,N'*-methylenebis(acrylamide) (BIS), acrylic acid, *N*-(3-aminopropyl) methacrylamide hydrochloride (APMA) (Polysciences), ammonium persulfate (APS), and sodium dodecyl sulfate (SDS) were used as received. All water used in the experiments was distilled, and then deionized using a Barnstead E-pure system operating at a resistance of 18 M Ω . A 0.2 μ m filter was used to remove

particulate matter. For folic acid conjugation, folic acid, 1-ethyl-3-methyl-(3-dimethylaminopropyl)carbodiimide (EDC) (Pierce), and dimethyl sulfoxide (DMSO) (Fisher) were used. The fluorescent monomer 4-acrylamidofluorescein (AFA) was synthesized via a previously reported procedure.³⁹

Nanogel Core Synthesis

Nanogel core/shell particles were synthesized by free-radical precipitation polymerization as reported previously.^{22, 23} For all particles, the molar composition of core particles was 96% NIPAm (or 96% NIPMAm), 2% BIS, and 2% AAc, or 98% NIPAm (or 98% NIPMAm), 2% BIS, and 0.1 mM AFA. A total monomer concentration of 70 mM was used for NIPAm particles, while a total concentration of 140 mM was used for NIPMAm particles. All polymerizations were carried out in a three-neck round bottom flask. As described below, various concentrations of SDS were used as the surfactant, and various concentrations of APS were used to initiate the reaction. In a typical synthesis, 100 mL of a filtered, aqueous solution of monomer, BIS, and SDS were added to the flask and heated to 70 °C. The solution was purged with N₂ gas and stirred vigorously until the temperature remained stable. The AAc was then added (where appropriate). After 15 minutes, the reaction was initiated by adding a 1 mL solution of the desired concentration of APS. The solution turned turbid, indicating successful initiation. The reaction was allowed to continue for 4 hours while being purged by N₂ gas with constant stirring. For particles containing AFA, the AFA was added along with the main monomer and cross-linker. After the synthesis, the solution was filtered through a Whatman filter paper. Conditions for all of the core syntheses can be found in Tables 1 and 2. For all syntheses, the batch to batch size variation was within 10%. Differences from batch to batch can simply be attributed to slight thermal fluctuations during the synthesis.

Nanogel Shell Synthesis

Core particles were used as seeds for the addition of a shell hydrogel. The detailed procedure of the shell synthesis has been reported in previous publications.^{22, 23} In brief, 10 mL of the core nanogel solution, 2 mM SDS, and 35 mL of deionized H₂O were added to a three-neck round bottom flask and heated under N₂ gas to 70 °C. Separately, a monomer mixture with the following molar ratios was dissolved in 5 mL of deionized H₂O: 97.5% NIPAm (or 97.5% NIPMAm), 2% BIS, and 0.5% APMA. This solution was added to the three-neck round bottom flask and heated to 70 °C. The reaction was initiated by a 1 mL solution of 0.5 mM APS and the reaction proceeded for four hours. Following the synthesis, the solution was filtered through a Whatman filter paper and then centrifuged several times for purification.

Particle Characterization

Static light scattering

Multi-angle laser light scattering (MALLS) (Wyatt Technology Corporation) detection following asymmetric field flow fractionation (AFFF) was used to determine the distribution of z-average radii (R_z) for all particles. The AFFF separation method uses a cross flow method to separate the particles as a function of hydrodynamic volume. The cross flow acts to force larger particles against a cellulose membrane, while smaller particles elute to the MALLS detector faster. For all separations, a cross flow of 0.5 mL/min was used. The MALLS detector is equipped with a Peltier device to maintain a flow cell temperature of 25 °C and collects scattered light from 16 different fixed angles to determine the R_z of the particles. By measuring R_z as a function of elution time, we construct a chromatogram that permits the determination of the weight fraction of particles as a function of radius, thereby providing a sample polydispersity. ASTRA 5.1.5.0 software was used to determine R_z values using the Debye fit method.

Fluorimetry

Particle LCST values were measured from turbidity curves collected on a steady-state fluorescence spectrophotometer (Photon Technology International), equipped with a Model 814 PMT photon-counting detector. Scattering was measured through slits that were set to attain a spectral bandwidth of 2 nm. The scattering was measured at a wavelength of 600 nm, and the temperature ramp was set from 25 °C to 60 °C. An integration time of 1 s was used and data was collected every 0.1 °C, with the temperature increasing at a rate of 1 °C per minute.

Folic acid conjugation

Nanogel core/shell particles were conjugated with folic acid by a method previously described by Dube et al.⁴⁰ The core/shell nanogel solution was freeze-dried and then resuspended in 40 mL of 10 mM phosphate buffer pH 4.7. A 2:1 molar ratio of folic acid to amine in the shell was dissolved in 1 mL DMSO. To this, a 2× equivalent of EDC was added to activate the folic acid. This solution was mixed for 15 minutes, and then added to the core/shell nanogel solution. The reaction was stirred in the dark overnight. The particles were then centrifuged/resuspended several times for purification.

Absorbance measurements

The absorbance of folic acid, core/shell particles, and folate-conjugated core/shell particles was determined using a Shimadzu UV 1601 spectrophotometer. Freeze-dried samples were dissolved in DMSO for absorbance measurements.

Results and Discussion

Table 1 shows the very straightforward progression we have followed in the synthesis of pNIPAm nanogels. These data show our ability to make core particles composed of p(NIPAm-co-acrylic acid), as well as pNIPAm core particles containing AFA as a fluorescent marker. For pNIPAm-co-AAc core particles, a 70 mM total monomer concentration was used for all reactions. The surfactant and initiator concentrations were gradually increased until the particle size approached the target 50-nm radius. As described above, MALLS coupled to the AFFF separation technique was used to characterize particle size and polydispersity. Examples of such data are shown in Figure 1, wherein highly monodisperse particle size distributions are evident from the differential weight fraction. Figure 1 also shows the overlay of the radius data with the raw detector signal, illustrating the high degree of monodispersity possible with these syntheses. The initial synthesis resulted in particles that were 86 nm in radius. This synthesis used 2 mM SDS and 2 mM APS. After increasing these concentrations to 3 mM each, the resulting particles were 73 nm in radius. Particles of appropriate size were synthesized when the SDS and APS concentrations were increased to 4 mM each. These particles had a radius of 53 nm. An interest in fluorescent tracking for future targeted chemotherapy studies led to our use of AFA as a co-monomer in the particle synthesis. Using the same synthesis conditions as described earlier, with the exception of 0.1 mM AFA being used instead of 2 % AAC, the particles slightly increased in size to 57 nm in radius, still close to the desired particle size. This data is shown in Figure 2. A further attempt to decrease the core particle size was successful, (Figure 3) where the particle size was further reduced in size to 44 nm in radius for pNIPAm-co-AFA. The decrease in size was achieved by increasing [BIS] and decreasing the total monomer concentration. Increasing the [BIS] caused the particles to be more highly cross-linked, resulting in the tighter, smaller particles. The reduction of total monomer concentration results in smaller particles due to the decreased amount of monomer that can be added during the polymerization.

Table 2 shows the synthetic progression for pNIPAm nanogel syntheses. The introductory synthesis used the same conditions as that of the successful pNIPAm synthesis. However, using

70 mM total monomer concentration did not result in good particle formation. This was most likely due to the lower propagation rate constant for NIPMAm versus NIPAm, which would result in slower particle nucleation.²⁹ The total monomer concentration was increased to 140 mM to achieve a successful synthesis. Since the synthesis required a higher monomer concentration, the surfactant and initiator concentrations had to be further increased to attain a particle size near 50 nm in radius. Figure 4 clearly shows that monodisperse particles can be made over a range of sizes using this straightforward synthetic approach. The progression of particle sizes is shown with error bars that denote the full width of the differential weight fraction, indicating very monodisperse particles obtained from each synthesis. The pNIPMAm syntheses were also performed using AFA, for fluorescent tracking, instead of acrylic acid as a co-monomer. Figure 4 shows these particles also had a slight increase (51 nm radius) over the acrylic acid particles, but were still close to 50 nm in radius. A further attempt to decrease the core particle size was also successful with pNIPMAm-co-AFA (pNIPMAm-co-AFA #6, Figure 4). The particle size was decreased to 45 nm by increasing [BIS] and decreasing the total monomer concentration.

A thin, hydrogel shell was added to the 57 nm-radius pNIPMAm-co-AFA core particles using a total monomer concentration of 20 mM in the feed solution. The shell consisted of pNIPAm, BIS, and APMA. The shell synthesis is a seeded precipitation polymerization reaction. The core particles are heated well above the LCST and the deswollen particles act as nuclei onto which growing polymer can be added. The thin shell compresses the core particle, and upon reswelling, the particle is actually smaller in size. Our group has previously shown shell compression, wherein the thin shell does not allow a complete reswelling of the core.²⁴ Figure 5 shows that the shell compression creates a particle that is 52 nm in radius, versus the 57 nm radius core. The addition of APMA incorporates primary amines in the shell to provide additional functionality to the particles.

In order to add a shell to the 51 nm-radius pNIPMAm-co-AFA core, the shell's monomer concentration had to be increased from that of pNIPAm, to 50 mM. The shell consisted of pNIPMAm, BIS, and APMA. With the increase in monomer concentration, the particles did not see a dramatic compression as with the pNIPAm particles. Compression of the core most likely still occurs, but the increase in monomer concentration (and hence the increase in shell thickness) was enough to overtake the amount of compression, and increase the total size of the particles. The pNIPMAm core/shell particles increased in size from 51 nm in radius for the core to 55 nm radius for the core/shell particles (Figure 6).

Figure 7 shows turbidity curves measured for both pNIPAm and pNIPMAm core/shell particles. The pNIPAm core/shell particles exhibited an LCST of ~ 31 °C, while the pNIPMAm core/shell particles exhibited an LCST of ~ 44 °C. Both of these values were as expected given the literature precedent referenced above. Future studies will compare targeting efficiencies of both sets of particles, as pNIPAm core/shell particles will be mainly deswollen at 37° C, while pNIPMAm core/shell particles will be mainly swollen at 37° C. The deswollen pNIPAm particles are hydrophobic, which can lead to the particles being taken up by the RES. The swollen pNIPMAm particles are hydrophilic, which may lead to avoidance of the RES and longer circulation times in the body.

The core/shell particles are suitable for bioconjugation due to the amines incorporated in the shell. A variety of bioconjugation strategies can be used to create targeting moieties on the shell of the particles using pendant amines.^{12, 41–43} In this case, we have used carbodiimide coupling to attach folic acid to the particles. Folic acid is biologically important, as it is needed by the body as vitamin B9. In addition, the folate receptor is overexpressed in many tumor cells. This makes folic acid and its receptor a prime candidate for targeting studies. Figure 8 shows the incorporation of folic acid on the core/shell particles. Particles were conjugated with

folic acid and cleaned several times by centrifugation to remove any free folic acid. Absorbance measurements for folic acid show a peak 285 nm. Unconjugated particles do not show this peak, while conjugated particles do show an absorbance peak at 285 nm, indicating folic acid has been conjugated to the particles. Future studies will use these bioconjugated core/shell particles for in vitro and in vivo targeting of cancer cells.

Conclusions

In this investigation, it has been shown that small, bioconjugated nanogels can be produced using a very straightforward synthetic approach. Through our synthetic methods, we have shown control over particle size, with the ability to synthesize a wide range of diameters. The particles are highly monodisperse at all sizes and core/shell compositions. The ability to incorporate acrylic acid in the core allows greater functionality among the particles (i.e. for additional chemoligations), while the AFA-incorporated core allows fluorescent tracking. The incorporation of amines in the shell gives the particles multiple functionalities, allowing simple conjugation to acid groups present on a number of biologically important targeting moieties. We have illustrated this ability with the addition of folic acid to the particles in this contribution. We are currently evaluating the efficacy of these particles as drug carriers, as their near-50 nm radii make them appropriate for intravenous delivery of therapeutics.

Acknowledgements

The authors acknowledge financial support from the DHHS (1 R21 EB006499-01) and the Emory-Georgia Tech Nanotechnology Center for Personalized and Predictive Oncology (5-40256-G11).

Abbreviations

NIPAm	N-isopropylacrylamide
LCST	lower critical solution temperature
NIPMAm	N-isopropylmethacrylamide
EPR	enhanced permeability and retention
RES	reticuloendothelial system
APS	ammonium persulfate
SDS	sodium dodecyl sulfate
BIS	<i>N, N'</i> -methylenebis(acrylamide)
APMA	<i>N</i> -(3-aminopropyl) methacrylamide hydrochloride
EDC	1-ethyl-3-methyl-(3-dimethylaminopropyl)carbodiimide

DMSO	dimethyl sulfoxide
AFA	4-acrylamidofluorescein
MALLS	multi-angle laser light scattering
AFFF	asymmetric field flow fractionation

References

1. Heskins M, Guillet JE. *J Macromol Sci Chem* 1968;A2:1441–1455.
2. Tanaka T. *Physica A* 1986;140A:261–268.
3. Tanaka T, Fillmore DJ. *J Chem Phys* 1979;70:1214–1218.
4. Tanaka T, Fillmore DJ, Sun S-T, Nishio I, Swislow G, Shah A. *Phys Rev Lett* 1980;45:1636–1639.
5. Schild HG. *Prog Polym Sci* 1992;17:163–249.
6. Kim S, Healy KE. *Biomacromolecules* 2003;4:1214–1223. [PubMed: 12959586]
7. Pelton RH, Chibante P. *Colloids Surf* 1986;20:247–256.
8. Lutolf MP, Raeber GP, Zisch AH, Tirelli N, Hubbell JA. *Adv Mater* 2003;15:888–892.
9. Langer R. *Nature* 1998;392:5–10. [PubMed: 9579855]
10. Langer R. *Acc Chem Res* 2000;33:94–101. [PubMed: 10673317]
11. Langer R. *Science* 2001;293:58–59. [PubMed: 11441170]
12. Nayak S, Lee H, Chmielewski J, Lyon LA. *J Am Chem Soc* 2004;126:10258–10259. [PubMed: 15315434]
13. Nayak S, Lyon LA. *Angew Chem Int Ed* 2005;44:7686–7708.
14. Kim J, Nayak S, Lyon LA. *J Am Chem Soc* 2005;127:9588–9592. [PubMed: 15984886]
15. Kim J, Serpe MJ, Lyon LA. *J Am Chem Soc* 2004;126:9512–9513. [PubMed: 15291534]
16. Holtz JH, Asher SA. *Nature* 1997;389:829–832. [PubMed: 9349814]
17. Plunkett KN, Berkowski KL, Moore JS. *Biomacromolecules* 2005;6:632–637. [PubMed: 15762623]
18. Pelton R. *Adv Coll Inter Sci* 2000;85:1–33.
19. Saunders BR, Vincent B. *Adv Coll Inter Sci* 1999;80:1–25.
20. Snowden MJ, Vincent B. *J Chem Soc, Chem Commun* 1992:1103–1105.
21. Zhou G, Elaissari A, Delair T, Pichot C. *Coll Polym Sci* 1998;276:1131–1139.
22. Gan D, Lyon LA. *J Am Chem Soc* 2001;123:7511–7517. [PubMed: 11480971]
23. Jones CD, Lyon LA. *Macromolecules* 2000;33:8301–8306.
24. Jones CD, Lyon LA. *Macromolecules* 2003;36:1988–1993.
25. Berndt I, Pedersen JS, Lindner P, Richtering W. *Prog Colloid & Polym Sci* 2006;133:35–40.
26. Berndt I, Popescu C, Wortmann F-J, Richtering W. *Angew Chem Int Ed* 2006;45:1081–1085.
27. Berndt I, Richtering W. *Macromolecules* 2003;36:8780–8785.
28. Duracher D, Elaissari A, Pichot C. *Coll Polym Sci* 1999;277:905–913.
29. Duracher D, Elaissari A, Pichot C. *J Polym Sci A Polym Chem* 1999;37:1823–1837.
30. Drummond DC, Meyer O, Hong K, Kirpotin DB, Papahadjopoulos D. *Pharmacol Rev* 1999;51:691–743. [PubMed: 10581328]
31. Hobbs SK, Monsky WL, Yuan F, Roberts WG, Griffith L, Torchilin VP, Jain RK. *Proc Natl Acad Sci* 1998;95:4607–4612. [PubMed: 9539785]
32. Yuan F, Dellian M, Fukumura D, Leunig M, Berk DA, Torchilin VP, Jain RK. *Cancer Res* 1995;55:3752–3756. [PubMed: 7641188]
33. Matsumura Y, Maeda H. *Cancer Res* 1986;46:6387–6392. [PubMed: 2946403]

34. Maeda H. *Adv Enzyme Regul* 2001;41:189–207. [PubMed: 11384745]
35. Maeda H, Seymour LW, Miyamoto Y. *Bioconjugate Chem* 1992;3:351–362.
36. Brannon-Peppas L, Blanchette JO. *Adv Drug Del Rev* 2004;56:1649–1659.
37. Storm G, Belliot SO, Daemen T, Lasic DD. *Adv Drug Del Rev* 1995;17:31–48.
38. Odian, G. *Principles of Polymerization*. 4. 2004.
39. Serpe MJ, Jones CD, Lyon LA. *Langmuir* 2003;19:8759–8764.
40. Dube D, Francis M, Leroux J-C, Winnik FM. *Bioconjugate Chem* 2002;13:685–692.
41. Leamon CP, Cooper SR, Hardee GE. *Bioconjugate Chem* 2003;14:738–747.
42. Leamon CP, Low PS. *Proc Natl Acad Sci* 1991;88:5572–5576. [PubMed: 2062838]
43. Leamon CP, Low PS. *Drug Discov Today* 2001;6:44–51. [PubMed: 11165172]

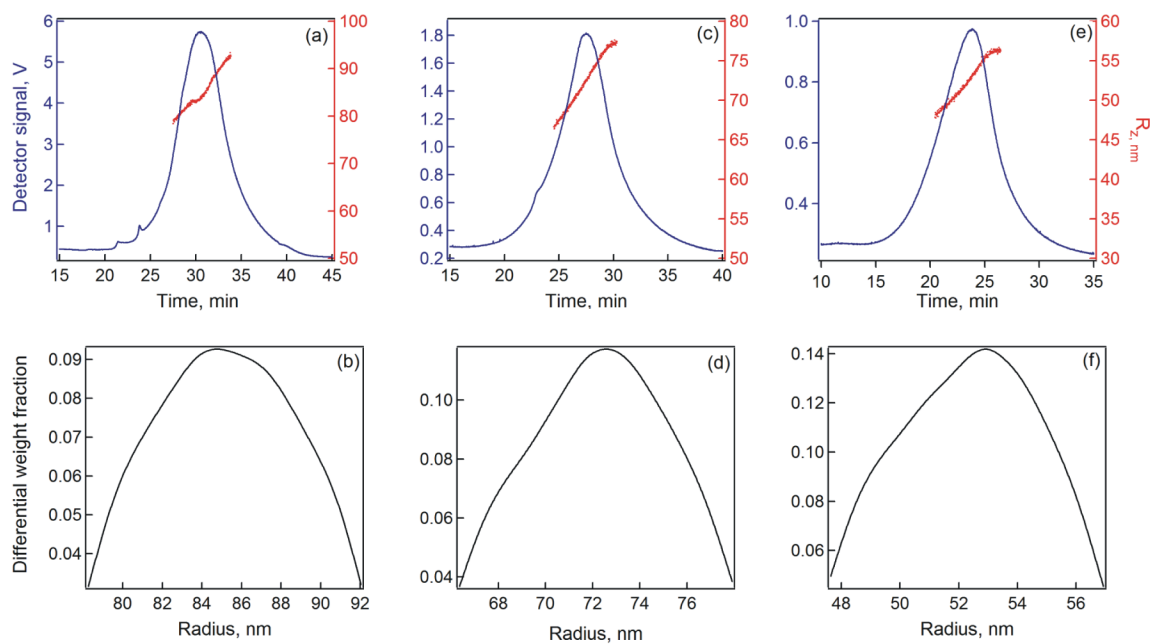


Figure 1.

Overlay of radius data as sample elutes to detector and is shown as voltage (a,c,e) for pNIPAm-co-AAc core particles, and corresponding differential weight fraction plots, as determined by AFFF-MALLS (b,d,f). Synthetic parameters for (a,b) are shown in Table 1, row 1; (c,d) are shown in Table 1, row 2; (e,f) are shown in Table 1, row 3.

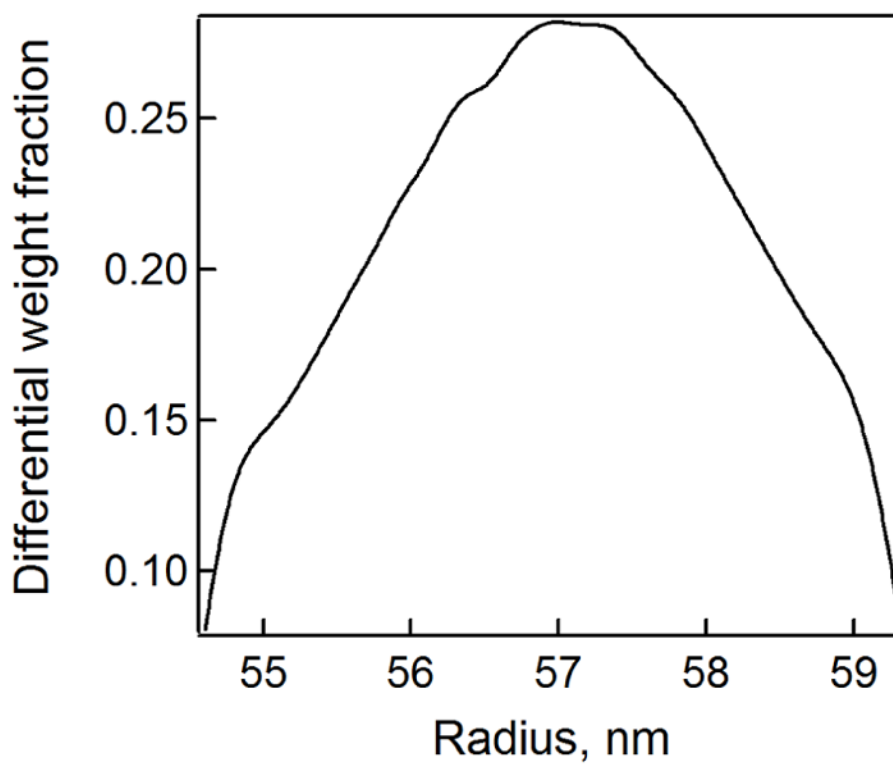


Figure 2. Differential weight fraction plot for pNIPAm-co-AFA core particles, as determined by AFFF-MALLS. Synthetic parameters are shown in Table 1, row 4.

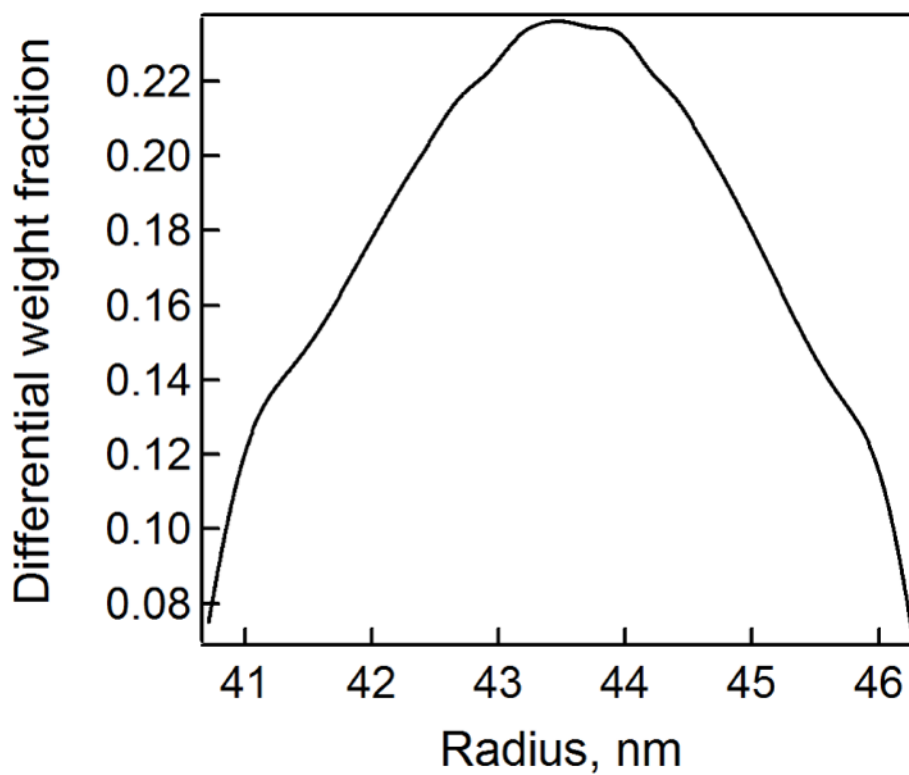


Figure 3. Differential weight fraction plots for pNIPAm-co-AFA core particles, as determined by AFFF-MALLS. Synthetic parameters are shown in Table 1, row 5.

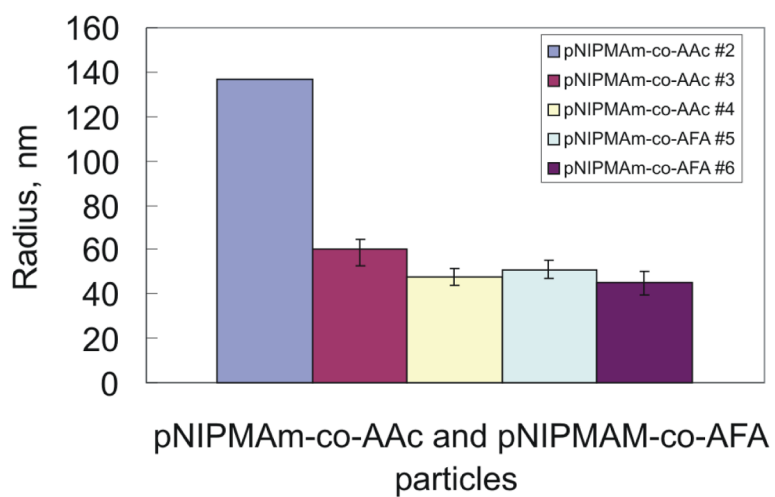


Figure 4. Particle sizes determined for the pNIPMAm core particle syntheses. Error bars do not indicate a standard deviation, but rather the total width of the differential weight fractions for each synthesis.

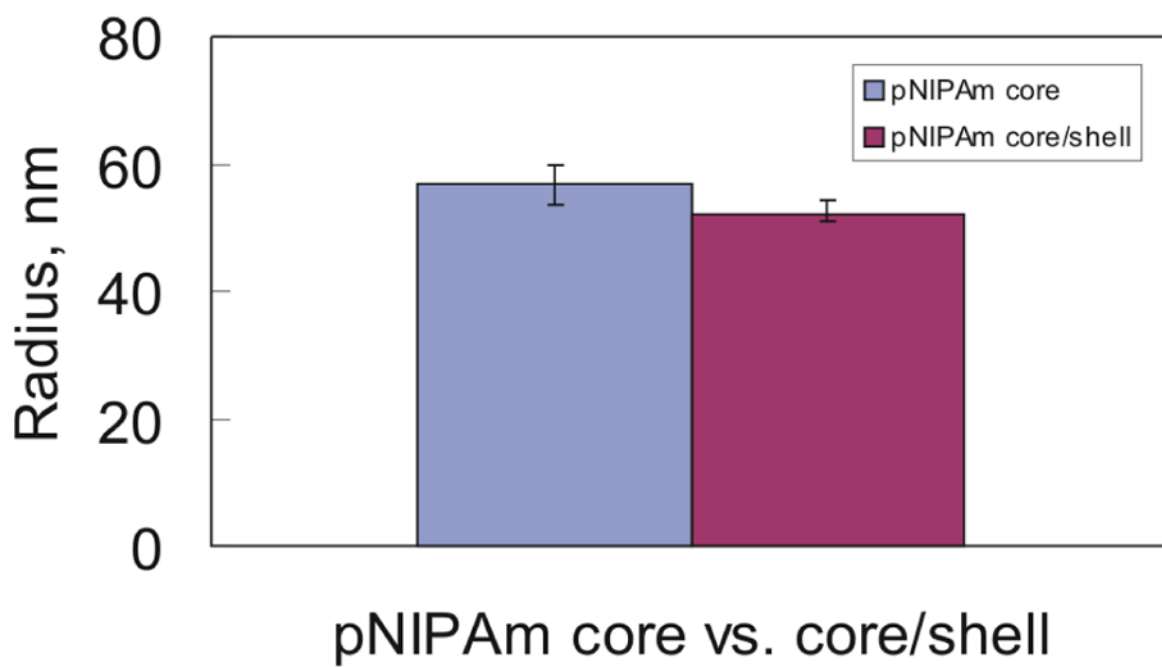


Figure 5. Change in size of pNIPAm core particles versus pNIPAm core/shell particles. Error bars indicate the total width of the differential weight fractions.

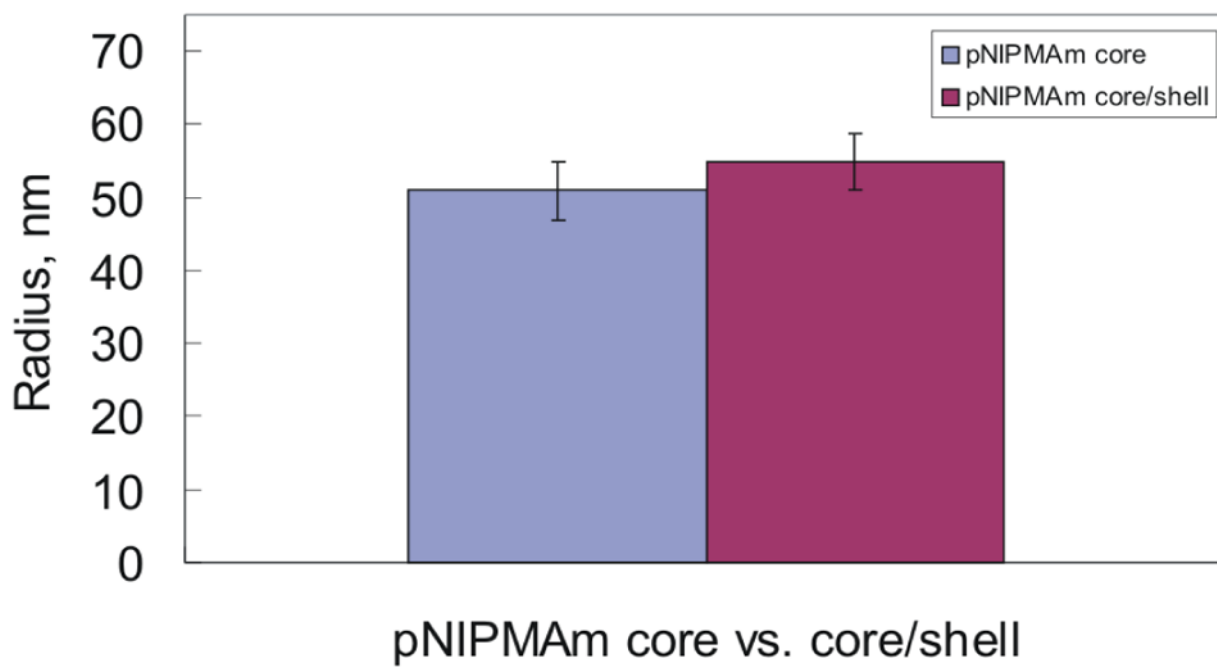


Figure 6. Change in size of pNIPMAm core particles versus pNIPMAm core/shell particles. Error bars indicate the total width of the differential weight fractions.

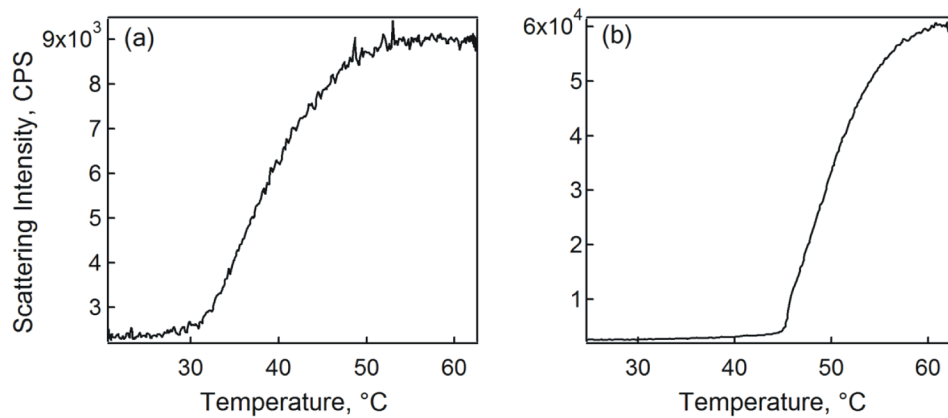


Figure 7. Temperature-dependent turbidity measurements for (a) pNIPAm core/shell particles and (b) pNIPMAM core/shell particles.

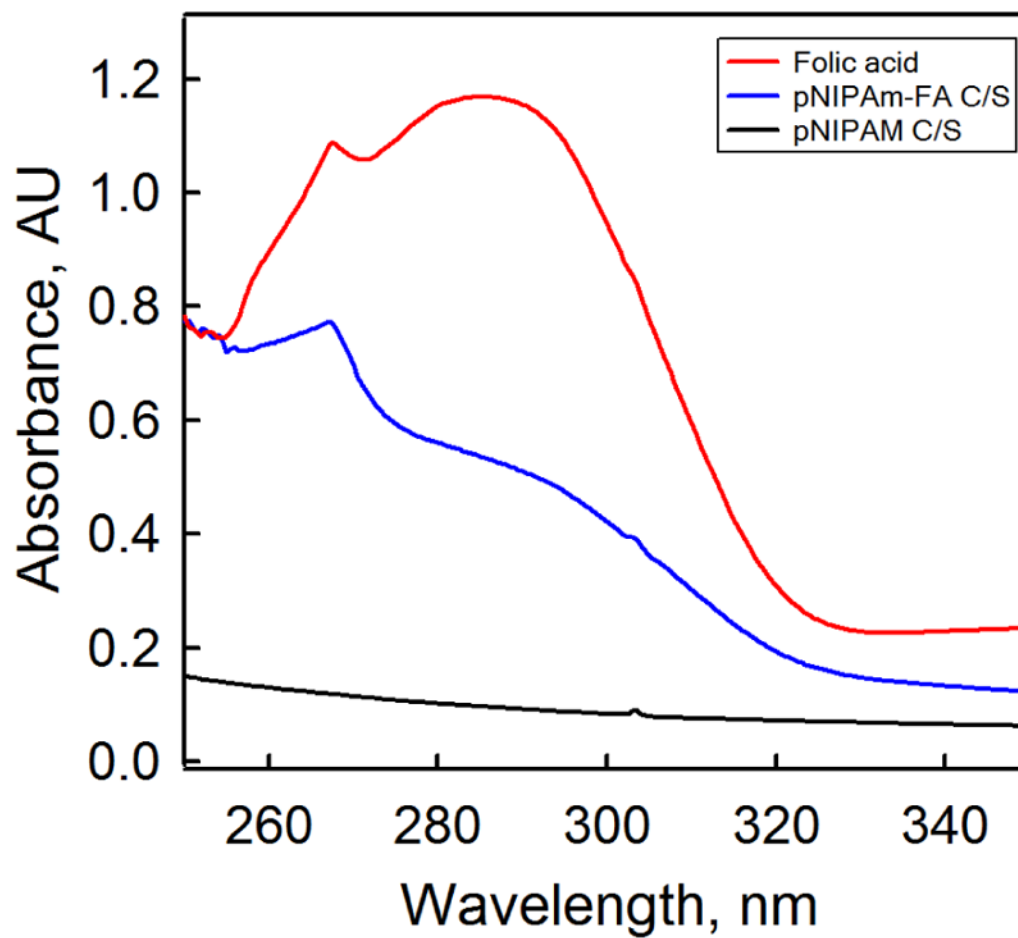


Figure 8. Absorbance of free folic acid (red), and pNIPAm core/shell particles before (black) and after (blue) folic acid conjugation.

Table 1

Parameters for pNIPAm core particle syntheses.

	Monomer	Cross-linker	Co-monomer	[Surfactant], mM	[Initiator], mM	[Total Monomer], mM	R_z , nm
1	pNIPAm- 96%	BIS- 2%	AAc- 2%	2	2	70	86
2	pNIPAm- 96%	BIS- 2%	AAc- 2%	3	3	70	73
3	pNIPAm- 96%	BIS- 2%	AAc- 2%	4	4	70	53
4	pNIPAm- 98%	BIS- 2%	AFA- 0.1 mM	4	4	70	57
5	pNIPAm- 95%	BIS- 5%	AFA- 0.1 mM	4	4	40	44

Table 2

Parameters for pNIPMAm core particle syntheses

	Monomer	Cross-linker	Co-monomer	[Surfactant], mM	[Initiator], mM	[Total Monomer], mM	R_p , nm
1	pNIPMAm- 96%	BIS- 2%	AAc- 2%	4	4	70	N/A
2	pNIPMAm- 96%	BIS- 2%	AAc- 2%	4	4	140	137
3	pNIPMAm- 96%	BIS- 2%	AAc- 2%	6	6	140	60
4	pNIPMAm- 96%	BIS- 2%	AAc- 2%	8	8	140	48
5	pNIPMAm- 98%	BIS- 2%	AFA- 0.1 mM	8	8	140	51
6	pNIPMAm- 95%	BIS- 5%	AFA- 0.1 mM	8	8	100	45